FULL PAPER

ADVANCED FUNCTIONAL MATERIALS

Nanocomposite Electrolytes with Fumed Silica and Hectorite Clay Networks: Passive versus Active Fillers**

By *Howard J. Walls*, *Michael W. Riley*, *Ruchi R. Singhal*, *Richard J. Spontak*, *Peter S. Fedkiw*, and *Saad A. Khan**

The use of nanocomposites constitutes a versatile and robust approach in the development of novel electrolytes with tailored electrochemical and mechanical characteristics. In this study, we examine the morphology, rheology, and ion-transport properties of two types of nanocomposite electrolyte gels, one consisting of branched silica nanoparticles and the other composed of hectorite clay. In the first system with hydrophobic (fumed) silica, oligomers of poly(ethylene oxide) (PEO), and lithium salt, the silica acts as a passive filler and does not participate in ion transport. The electrochemical properties are controlled by the salt–PEO electrolyte, allowing for ionic conductivities greater than 10^{-3} S cm^{-1} at ambient temperature. At sufficiently high concentrations, the silica forms an elastic gel possessing a large open network structure that provides for unimpeded ion mobility. In the second system composed of lithium-exchanged hectorite filler, the nanoscale platelets serve as the anion. This active filler yields ionic conductivities in excess of 10^{-4} S cm^{-1} and lithium transference numbers approaching unity. Similar to fumed silica, the hectorite clay also forms an elastic gel network. However, the morphologies of the two systems are distinctively different both in terms of network structure and characteristic length scale. These morphological differences manifest themselves in different rheological responses with regard to gel modulus and yield stress.

1. Introduction

The development of solid polymer electrolytes is recognized as a viable solution to many of the problems currently faced by rechargeable lithium (Li) and lithium-ion batteries. Polymer electrolytes derived principally from Li salts dispersed in poly(ethylene oxide) (PEO) promise improved safety and reliability, better electrode–electrolyte stability, and excellent mechanical stability.[1–6] Moreover, they may eliminate the need for separators and can conform to any cell shape that an application may require, thereby avoiding can-type design constraints.[5–7] However, development of a solid polymer electrolyte with desirable properties that include high ambient-temperature conductivity, high Li transference number (i.e., high mobility of lithium cation relative to anion), mechanical stability, and processability, is yet to be realized.[5,8] This is because many of these properties are mutually exclusive, in which case efforts to improve one, such as conductivity, may only be achieved at the expense of other properties, such as reduced mechanical strength.[1,3–5]

An intriguing and facile approach to address the shortcoming of low conductivity involves the addition of inorganic fillers (e.g., SiO_2 or Al_2O_3) to PEO-based electrolytes.[1,4,9] Addition of micro-/nanoscale particulates to such electrolytes to form hybrid nanocomposites results in an increase in conductivity, a slight increase in Li transference number, improved electrode–electrolyte interfacial stability, and little compromise in mechanical strength.[1,4,9–14] The reported increase in conductivity reflects the ability of the particles to inhibit crystallization of high-molecular-weight PEO and, consequently, promote polymer mobility.[11,12,15] Improved Li transference numbers have been attributed to the role of the ceramics, which serve as Lewis acid–base centers that effectively increase the number of free Li cations.[14] Unfortunately, the conductivity improvement in these systems is not sufficient to warrant their usage in commercial applications. Since the particulates employed in these systems are not charged and play no direct role in ion transport, we refer to them as "passive" fillers. A related approach to improve the performance of polymer electrolytes by enhancing the Li transference number uses Li-exchanged nanoclays (e.g., hectorite, laponite, and montmorillonite) in a polymer (e.g., PEO) capable of solvating Li cations.[16–19] In this regard, PEO molecules intercalate within the galleries of the organoclay platelets and solvate the Li cations. The large clay platelets therefore serve as anions, but have low mobility because of their size. As such, high Li transference numbers can be expected. Unfortunately, low ionic conductivity is typically observed in these materials, even after they are further doped with a salt such as lithium triflate ($LiCF_3SO_3$).[16–18] Since the Li-exchanged organoclays used in these systems directly affect ion transport, we refer to them as "active" fillers.

The ability of an electrolyte to transport ions is strongly coupled to i) its ability to solvate/dissociate a salt and ii) the resultant mobility of the ions in the electrolyte.[4,5,20–22] In PEO-based electrolytes, the polar ether linkages coordinate

[*] Prof. S. A. Khan, Dr. H. J. Walls,[+] Dr. M. W. Riley,[++] R. R. Singhal, Prof. R. J. Spontak, Prof. P. S. Fedkiw
Dept. of Chemical Engineering, North Carolina State University
Raleigh, NC 27695-7905 (USA)
E-mail: khan@eos.ncsu.edu

[+] Present address: Polymers Division, National Institute of Standards and Technology, Gaithersburg, MD 20899-8542, USA.

[++] Present address: Micro Cell Corp., Raleigh, NC 27606, USA.

[**] The authors gratefully acknowledge the U.S. Department of Energy (BES and BATT) for its support of this work. This work has also been funded, in part, by the NCSU Hoechst-Kenan program and the Air Force Office of Scientific Research through the U.S. DoD National Defense Science and Engineering Fellowship Program.

  DOI: 10.1002/adfm.200304333 *Adv. Funct. Mater.* **2003**, *13*, No. 9, September

ADVANCED FUNCTIONAL MATERIALS

the cations, while a large low-lattice energy anion delocalizes the negative charge.[4,5,21] The ions then migrate through the amorphous regions of the polymer matrix as a result of local segmental motion. Increasing the chain mobility generally induces an increase in conductivity.[3,21] Electrolytes with a high dielectric constant and low viscosity can yield very high ion transport.[5,23] This design paradigm explains why carbonates such as ethylene carbonate (EC) and dimethyl carbonate are common solvents used in commercial Li ion batteries.[5–7] In similar fashion, a marked increase in conductivity is found to occur in PEO-based electrolytes when the molecular weight of PEO (M_{PEO}) falls below the critical molecular weight of entanglement ($M_e \sim 3200\ g\,mol^{-1}$).[24] Low-molecular-weight PEO with $M_{PEO} < 500\ g\,mol^{-1}$, often referred to as poly(ethylene glycol) (PEG), is molten at ambient temperature, and possesses a relatively low melt viscosity to promote high ion transport. The drawback to using low-molecular-weight PEO is that it is a liquid at ambient temperature rather than the desired mechanically stable solid.

Our effort to formulate nanocomposite electrolytes, which deviates significantly from the traditional approach, exploits the high ambient temperature ionic conductivity possible in PEG or mixtures of PEG and carbonates, and uses nanoscale particulates that can form a three-dimensional network structure to impart mechanical stability. In this regard, we consider two types of fillers: a passive fumed silica that forms a branch-like network and an active Li-exchanged hectorite clay with a high aspect ratio. Electrolytes derived from fumed silica consist of PEG dimethyl ether (PEGdm), a Li salt such as lithium bis(trifluoromethanesulfonyl)imide (LiTFSI), and a fumed silica modified with various surface groups such as hydrophobic C_8H_{17}.[25–27] When a sufficient amount of fumed silica is dispersed in the liquid PEGdm–LiTFSI electrolyte, the fumed silica organizes into a three-dimensional network that provides the requisite mechanical strength through physical gelation[26,28] while retaining favorable ion transport with an ionic conductivity (σ) in excess of $10^{-3}\ S\,cm^{-1}$ at ambient temperature.[29] While the mechanical properties of such nanocomposites are primarily governed by the fumed silica,[26] ion transport is dictated by the PEGdm–LiTFSI matrix. In contrast, nanocomposites derived from hectorite are formed by dispersing Li-exchanged synthetic hectorite in a mixture of EC and either PEGdm or propylene carbonate (PC). Since the hectorite serves the dual role as anion and network-forming filler, high Li transference numbers and mechanical strength are simultaneously realized.[30] In this case, the mixed EC/PEGdm or EC/PC solvent provides for relatively high ion transport at ambient temperature with $\sigma > 10^{-4}\ S\,cm^{-1}$.

Previous work on these nanocomposites have addressed some aspects of their electrochemistry[29,30] and rheology.[26,28] Missing, however, is a detailed morphological analysis of these systems together with a comprehensive understanding of the relationship between observed morphology, electrochemistry, and rheology. Such an understanding is essential in establishing new design paradigms for nanocomposite electrolytes. In this study, we investigate and compare the morphologies and properties of passive and active routes to efficient nanocomposite electrolytes for Li-ion battery applications. On one hand, the fumed silica serves as an inert filler that improves mechanical strength with little influence on ion transport. On the other hand, Li-exchanged hectorite constitutes an active filler that benefits both mechanical strength and Li transference number.

2. Results and Discussion

2.1. Fumed Silica Nanocomposite Electrolytes

Addition of hydrophobic fumed silica to the liquid electrolyte composed of PEGdm and LiTFSI salt creates an elastic network, the dynamic rheology of which is presented in Figure 1. Figure 1a, which is representative of the dynamic elastic (G') and viscous (G'') moduli as functions of frequency (ω), clearly reveals that G' is i) much larger in magnitude than G'' and ii) relatively independent of frequency. These characteristics taken together confirm that a self-supporting three-dimensional network structure composed of the fumed silica filler develops. In this case, the nanocomposite behaves as a physical gel. Figure 1b shows the elastic and viscous moduli as functions of increasing stress amplitude (τ) for the same nanocomposite

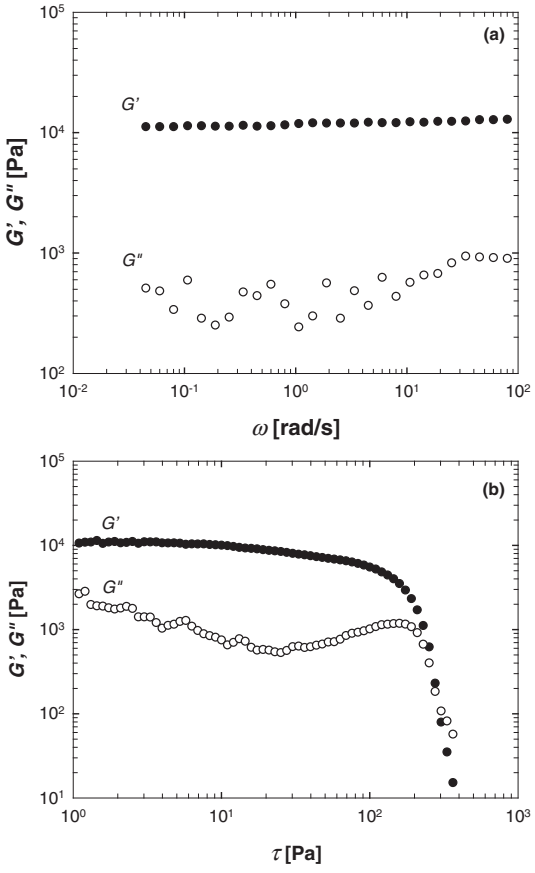

Fig. 1. Dynamic elastic (G') and viscous (G'') moduli as functions of frequency (a) and stress (b) for a typical nanocomposite electrolyte derived from fumed silica. The data correspond to a nanocomposite with 1.06 M (Li/O = 1:20) LiTFSI salt in PEGdm and 7 wt.-% octyl modified (R805) fumed silica evaluated at 30 °C. The frequency test in (a) has been conducted at a stress amplitude of 3.5 Pa, whereas the test in (b) has been conducted at a frequency of 1 rad s^{-1}.

electrolyte. At low stresses, the elastic modulus G' is larger than the viscous modulus G'' and relatively independent of stress, characteristic of the behavior of a gel in the linear viscoelastic (LVE) regime.[31] However, with increasing stress, the elastic modulus decreases precipitously above a critical stress of ~ 100 Pa. In addition, G' becomes smaller in magnitude than G''. These observations indicate that the physical association of fumed silica particles starts to deteriorate beyond a critical stress and the network structure breaks down (yields) so that the material is able to flow freely.

The effect of fumed silica content on the elastic modulus (G') and yield stress (τ_y) for a 1.06 M nanocomposite electrolyte (O/Li = 20) is provided for illustrative purposes in Figure 2. As silica is added to the system, more physical linkages are formed, thereby promoting a substantial increase in the gel modulus. The stress required to disrupt the network, i.e., the yield stress, also increases considerably with silica volume fraction (ϕ). It is noteworthy that both G' and τ_y exhibit power-law dependence on ϕ, i.e., G' or $\tau_y \sim \phi^n$; for G', n is 3.2, and for τ_y, n is 3.0. These results demonstrate that the addition of an inert, hydrophobic fumed silica can dramatically and controllably alter the rheological properties of a polymer electrolyte, resulting in an elastic solid that is yet processable.

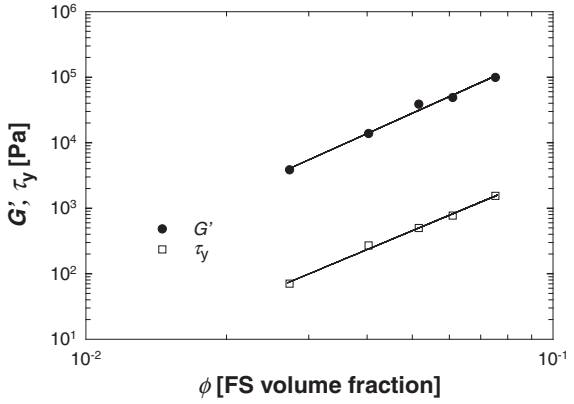

Fig. 2. Dependence of the elastic modulus (G') and yield stress (τ_y) on fumed silica volume fraction (ϕ). The data correspond to a nanocomposite electrolyte with 1.06 M (Li/O = 1:20) LiTFSI in PEGdm and octyl-modified (R805) fumed silica evaluated at 30 °C. The solid lines correspond to power-law fits to the data.

While the data presented in Figures 1,2 indicate that the rheological properties of the fumed silica nanocomposite electrolytes are strongly dependent on silica concentration, the electrochemical properties of these electrolytes are not. Figure 3 shows the conductivity (σ) and the Li transference number (T_{Li}) for a 1.06 M electrolyte as a function of fumed silica content. In this example, σ decreases by only 14 % upon addition of nearly 160 g silica per liter PEGdm. Even in light of this modest reduction, σ remains above the desirable value of 10^{-3} S cm^{-1} over the entire filler concentration range explored. Furthermore, Figure 3 demonstrates that T_{Li} increases slightly (which is beneficial) upon addition of fumed silica. Comparison of Figures 2 and 3 indicates that the mechanical and electrochemical properties of these fumed silica nanocomposite electrolytes are not coupled, in which case these properties can be independently tuned to satisfy application requirements.

To elucidate the mechanism by which fumed silica imparts favorable macroscopic properties—high ionic conductivity and mechanical stiffness—to these nanocomposite electrolytes, we have investigated their morphologies by transmission electron microscopy (TEM). As alluded to in the Experimental section (Sec. 4), difficulties associated with microtoming/stabilizing ultrathin sections (ca. 50–70 nm thick) of Aerosil R805/PEGdm systems have been alleviated by using a cross-linkable analog composed of Aerosil R711 and a mixture of PEGdm and PEG diacrylate (PEGda), in which the fraction of PEGda was varied from 20 to 100 wt %. Relatively low magnification energy-filtered TEM images of these nanocomposite electrolytes, acquired at two different electron energy loss (ΔE) settings, are displayed for comparison in Figure 4. Those shown in Fig-

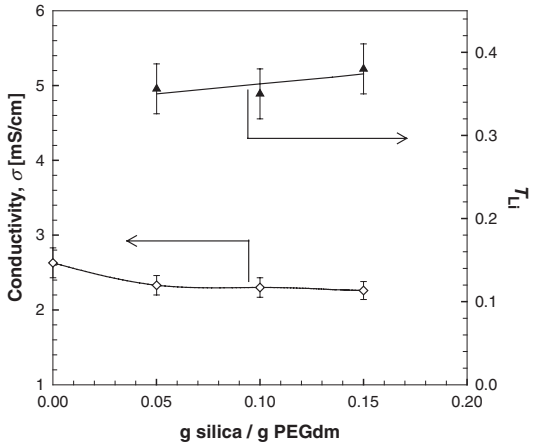

Fig. 3. Variation of ionic conductivity (σ) and Li transference number (T_{Li}) with fumed silica concentration. These data correspond to a nanocomposite electrolyte with 1.06 M (Li/O = 1:20) LiTFSI in PEGdm and R805 fumed silica evaluated at 30 °C. Error bars denote one standard deviation in the data, and the solid lines serve as guides for the eye.

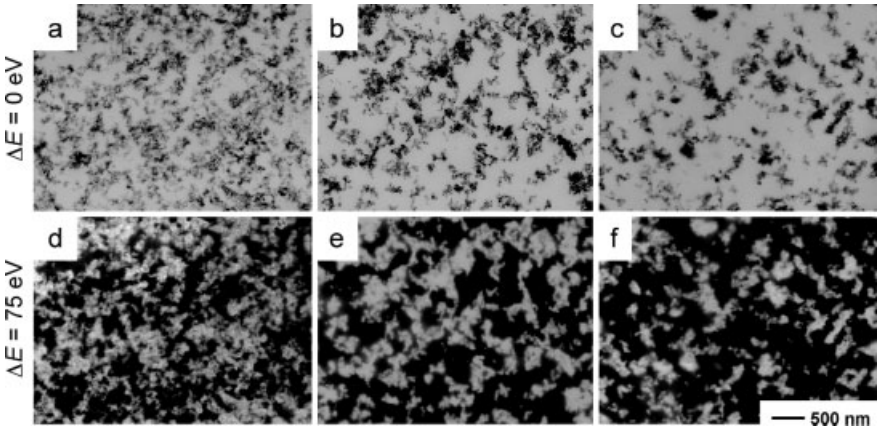

Fig. 4. Energy-filtered TEM images obtained from fumed silica nanocomposite electrolytes with different concentrations of PEGda (in wt.-%) in the PEGdm/PEGda solvent mixture: a,d) 100, b,e) 66, and c,f) 20. Images displayed in (a–c) have been acquired at an electron energy loss (ΔE) of 0 eV, whereas those shown in (d–f) have been collected at ΔE = 75 eV and confirm the presence of non-carbonaceous features (light).

ures 4a–c have been collected at $\Delta E = 0$ eV, which means that image formation occurs primarily by elastically and non-scattered electrons. Inelastically scattered electrons possessing a ΔE greater than ca. 30 eV (the width of the energy filter) are excluded from these so-called "zero-loss" images.[32] Conversely, the matched images provided in Figures 4d–f have been obtained at $\Delta E = 75$ eV and clearly identify the structural characteristics that are non-carbonaceous (i.e., the fumed silica). Ideally, "structure-sensitive" imaging such as this should be conducted at higher ΔE (below the ionization edge of carbon at $\Delta E = 284$ eV) to minimize collection of electrons inelastically scattered from carbon during image formation,[32,33] but illumination considerations precluded imaging at higher ΔE settings. Structure-sensitive images provide greater contrast between carbonaceous and non-carbonaceous species than conventional TEM images. For this reason, this imaging mechanism is particularly useful in the morphological study[34] of organic/inorganic nanocomposites.

The images included in Figure 4 illustrate the effect of varying the fraction of PEGda in the mixed PEGdm/PEGda solvent. At all three PEGda concentrations examined, individual fumed silica particles appear to form a highly branched morphology possessing high interfacial area. This feature is responsible for the substantial change in rheological properties observed in Figure 2 and elsewhere at relatively small filler concentrations. Note from the images in Figure 4 that the fumed silica is the most dispersed as small aggregates and individual particles in Figures 4a,d, in which the electrolyte solvent is 100 wt.-% PEGda. As the fraction of PEGda in the solvent is reduced in Figures 4b,e and 4c,f, the fumed silica particles are observed to form larger aggregates and a generally more open branched morphology. This observation can be attributed to the ability of PEGda to form chemical cross-links in the polymer matrix and permanently lock-in the fumed silica morphology before it is capable of organizing into large-scale structural elements. Decreasing the fraction of PEGda in the solvent slows the rate, as well as lowers the extent, of polymer cross-linking, thereby allowing greater flocculation of fumed silica particles.

The particulate networks formed by fumed silica in Figure 4 and, at higher magnification in, Figure 5, are responsible for imparting mechanical stability to these nanocomposite electrolytes. While the images displayed in Figures 4,5 are two-dimensional, it must be remembered that the networks are three-dimensional in nature, forming an inorganic skeleton within an organic matrix, as can be seen by some of the faint features evident in Figure 5b. Despite noticeable structural differences in these images due to varying PEGda fraction, all the networks are, for the most part, open, with "pore" sizes increasing with increasing fumed silica flocculation. These pores permit relatively unhindered migration of ionic species throughout the polymer matrix, which explains why both σ and T_{Li} are weakly dependent on fumed silica concentration (see Fig. 3). Since the polymer matrix employed in the rheological and electrochemical tests discussed thus far consists exclusively of PEGdm, we expect that the fumed silica networks in those nanocomposite electrolytes more closely resemble Figures 4c,f and 5c than any of the other images in Figures 4,5.

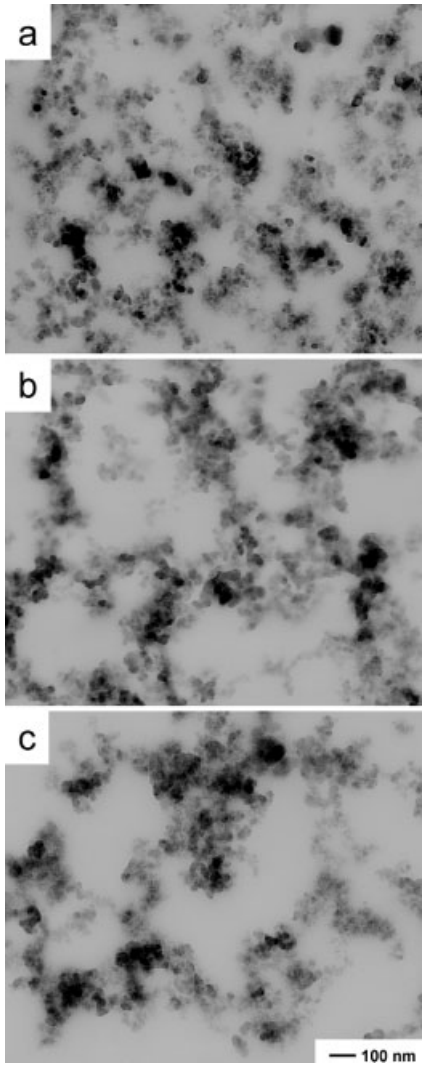

Fig. 5. Zero-loss TEM images of fumed silica nanocomposite electrolytes with varying concentrations of PEGda (in wt.-%) in the PEGdm/PEGda solvent mixture: a) 100, b) 66, and c) 20.

2.2. Hectorite Nanocomposite Electrolytes

When hectorite is properly dispersed in a solvent mixture of EC and either PEGdm or PC, it likewise forms a physical gel. Dynamic rheological results obtained from a typical nanocomposite electrolyte derived from hectorite are presented in Figure 6. The electrolyte employed in these tests consists of 120 g clay per liter of solvent in a 1:1 v/v mixture of EC and PEGdm. For convenience sake, the rheology experiments have been performed with native Na–hectorite, rather than Li-exchanged hectorite, since the alkali counterion is not expected to alter the rheological properties of these materials to any measurable extent. Since G' in Figure 6a is i) consistently larger than G'' over 3 orders of magnitude in frequency and ii) relatively independent of frequency, we conclude that this nanocomposite electrolyte behaves as a physical gel. Figure 6b shows the variation in G' with respect to stress and reveals the

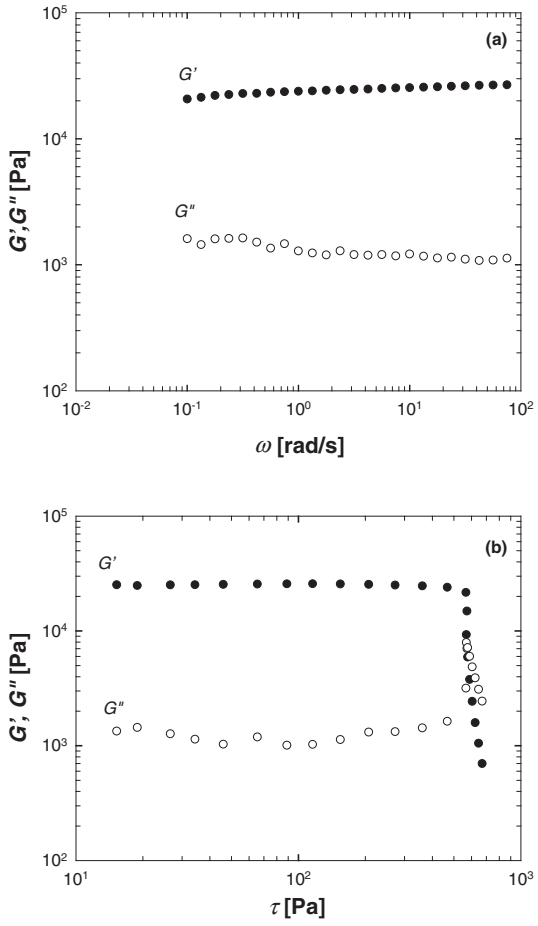

Fig. 6. Dynamic elastic (G') and viscous (G'') moduli as functions of frequency (a) and stress (b) for a typical nanocomposite electrolyte derived from native Na–hectorite. The data correspond to a specimen with 120 g clay per liter of solvent (1:1 v/v EC/PEGdm) evaluated at ambient temperature (~25 °C). The test in (a) has been conducted at stress amplitude of 3.5 Pa, whereas the test in (b) has been conducted at a frequency of 1 rad s^{-1}.

existence of a critical stress at ~600 Pa. Note that the magnitude of this critical stress is significantly higher than that measured for the fumed silica nanocomposite in Figure 1b.

Another interesting difference between the dynamic stress data provided here is that the critical stress of the clay-based nanocomposite (Fig. 6b) is better defined than that of the fumed silica nanocomposite (Fig. 1b). This difference is attributed to the shape of the primary particles, as well as the resulting network that forms upon flocculation. In the case of fumed silica, the primary particles are irregular in shape, but can be envisaged as roughly spherical. Hectorites, however, are platelet-like with a high aspect ratio (~250:1 for the hectorite used here). When the fumed silica nanocomposite is subjected to shear, the network is gradually disrupted due to the existence of numerous branch points (differing in size and location) that must break and disentangle before the material can flow. In marked contrast, increasing the shear stress serves to align the high-aspect-ratio platelets in the hectorite nanocomposite. Once sufficient stress is applied, the hectorite platelets abruptly slip past each other, thereby allowing the material to flow freely.

Analogous to the silica-based nanocomposite electrolytes, the gel modulus and yield stress for the hectorite nanocomposites in EC/PEGdm also exhibit a power-law dependence with respect to filler loading (Fig. 7). However, the power-law exponents for both G', $n = 9.1$, and τ_y, $n = 7.9$, are larger for the clay system relative to the corresponding exponents for the silica nanocomposite. Accordingly, the G' data in Figure 7 increases by almost two orders of magnitude as the concentration of Na–hectorite increases by less than a factor of two. A comparable increase in G' measured from the fumed silica nanocomposites requires nearly a three-fold increase in fumed silica concentration. Moreover, the physical gels formed by the hectorite have considerably higher elastic moduli than those formed by fumed silica. In fact, the Na–hectorite nanocomposites tested by rheology (see Figs. 6,7) are at least half as concentrated as those employed in the subsequent conductivity and morphological analyses.

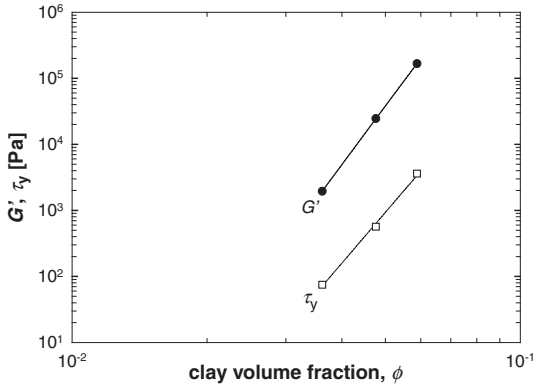

Fig. 7. Effect of Na–hectorite volume fraction (ϕ) on elastic modulus (G') and yield stress (τ_y) at ambient temperature (~25 °C). The solvent is 1:1 v/v EC/PEGdm. The solid lines represent power-law fits to the data.

The effect of Li–hectorite concentration on conductivity (σ) is presented in Figure 8. As with the nanocomposite electro-

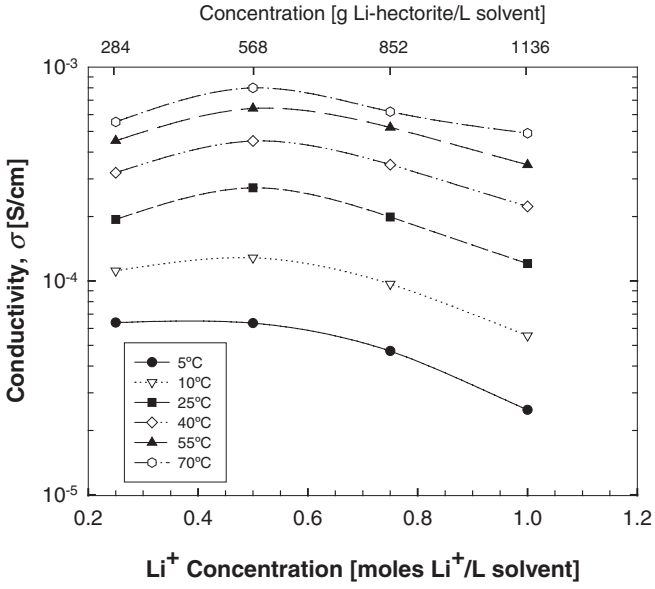

Fig. 8. Variation of conductivity (σ) with Li–hectorite concentration at several different temperatures. The solvent is 1:1 v/v EC/PEGdm. The solid lines serve as guides for the eye.

ADVANCED FUNCTIONAL MATERIALS

lytes derived from fumed silica (see Fig. 3), σ values in excess of 10^{-4} S cm^{-1} are achieved over the entire range of filler concentrations explored at ambient temperature and above. While the standard that has been established for the conductivity of solid electrolytes to be commercially competitive is 10^{-3} S cm^{-1}, theoretical considerations[8] suggest that electrolytes with T_{Li} approaching unity could tolerate σ values as low as 10^{-4} S cm^{-1}. It is important to recognize that batteries with $T_{Li} = 1.0$ would be particularly useful for high-discharge applications since they would be less susceptible to deleterious effects arising from concentration polarization.[8,35] Riley et al.[30] have measured T_{Li} values as high as 0.98 for Li–hectorite in PC.

High-resolution imaging of these hectorite nanocomposite electrolytes can reveal both the bulk dispersion of the clay within the solvent matrix and the degree to which the clay is intercalated or exfoliated. We first consider the dispersion of the hectorites dispersed in EC/PEGda for the same reasons discussed earlier with regard to fumed silica (Figs. 4,5). Figure 9 shows energy-filtered TEM images of nanocomposites at two different hectorite concentrations and two different ΔE values.

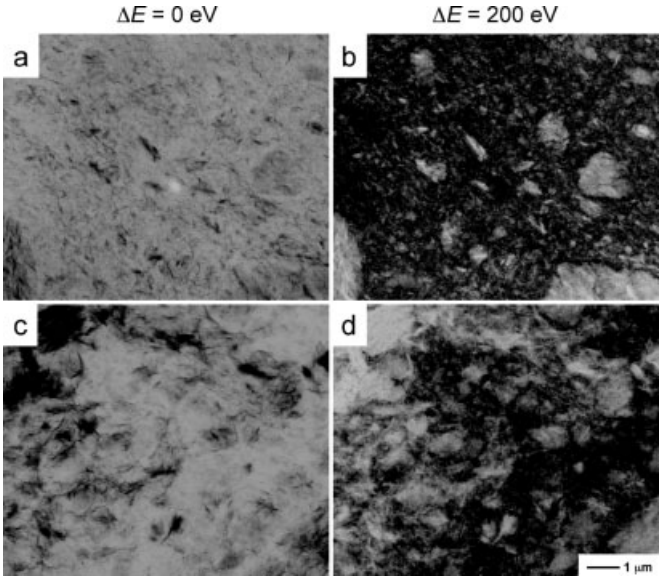

Fig. 9. Energy-filtered TEM images acquired from Li–hectorite nanocomposite electrolytes with different concentrations of Li–hectorite (in M) in EC/PEGda: a,b) 0.25 and c,d) 0.50. Images displayed in (a,c) have been obtained at $\Delta E = 0$ eV, whereas those in (b,d) have been collected at $\Delta E = 200$ eV to elucidate the spatial distribution of the organoclay (light).

The non-carbonaceous hectorite platelets are more clearly visible in the structure-sensitive images acquired at $\Delta E = 200$ eV. Many of the platelets measure ~1 μm across, and the spacing between platelets (or platelet aggregates) appears generally smaller in the nanocomposite with the higher hectorite concentration. The morphologies evident in these images indicate reasonably good clay distribution, but are less uniform and more aggregated than those obtained from fumed silica in Figure 4. This observation may explain why the hectorite nanocomposite electrolytes are stiffer than those prepared with fumed silica (see Figs. 2,7). Another noteworthy feature of Figure 9 is that the orientation of the hectorite platelets appears random, which is expected to yield isotropic bulk (mechanical and conductivity) properties. Under large amplitude strain, however, the platelets will preferentially align and exhibit a propensity to flow, as observed in Figure 6b. It is expected that upon cessation of shear, the hectorite platelets will again orient randomly in a pseudo-solid state.[36]

Evidence of intercalation or exfoliation depends on the orientation of the platelets relative to the electron beam, and the degree to which the platelets are exfoliated or intercalated, can only be ascertained if the platelets are aligned edge-on. Figure 10 displays a series of TEM images acquired from Li–hectorite nanocomposites at two concentrations dispersed in EC/PEGda. These images show platelets that are oriented

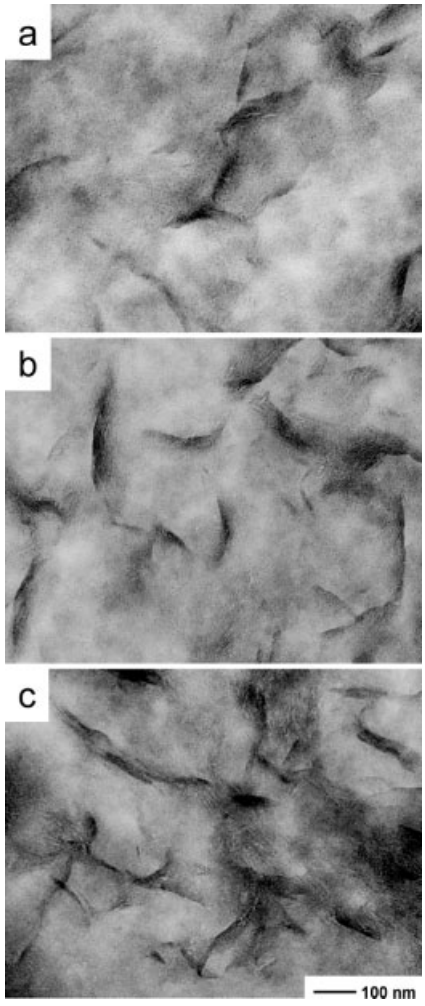

Fig. 10. Zero-loss TEM images of Li–hectorite nanocomposite electrolytes with different concentrations of Li–hectorite (in M) in EC/PEGda: a,b) 0.75 and c) 1.00.

edge-on and reveal the existence of small, thin bundles measuring 8–12 nm thick, which translates into 2–3 platelets if each platelet is about 4 nm thick.[37] Indeed, individual platelets measuring ca. 4 nm thick are visible in Figure 11. The images provided in Figures 10,11 confirm that most of the hectorite platelets are intercalated, rather than exfoliated. The extent to which the platelets are intercalated or exfoliated is expected to

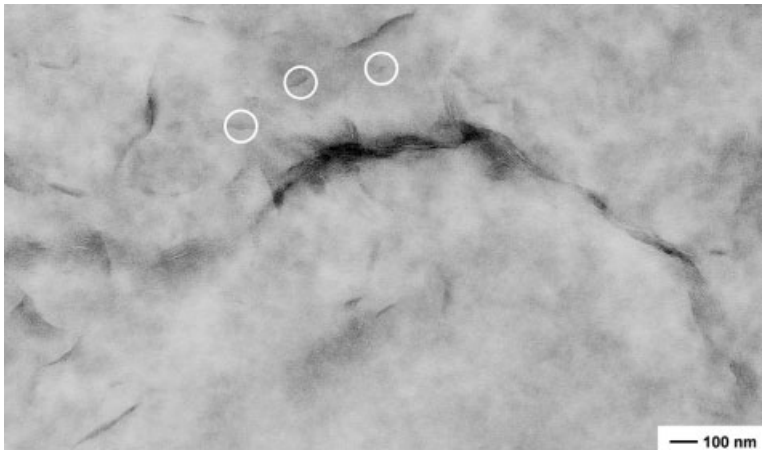

Fig. 11. Energy-filtered TEM image ($\Delta E = 0$ eV) of a nanocomposite electrolyte with 0.75 M Li-exchanged hectorite dispersed in EC/PEGda. The circled regions identify single exfoliated hectorite platelets.

play a distinct role in the conductivity of these nanocomposite electrolytes. A completely exfoliated morphology is expected to yield the highest σ since more Li cations would be mobile and available for conduction. Conversely, a system in which the Li cations are "trapped" between intercalated platelets would not be nearly as conductive. Likewise, the rheological behavior of these nanocomposites should be directly linked to the dispersion of the hectorite platelets, with complete exfoliation yielding a larger gel modulus, as well as inducing gelation at lower concentrations.

3. Conclusion

In this study, two strategies for producing nanocomposite electrolytes, one employing a passive fumed silica filler and the other using an active Li–hectorite filler, are examined. Both approaches yield elastic gels exhibiting ionic conductivities in excess of 10^{-4} S cm^{-1}. In the case of hydrophobic fumed silica, the filler forms an open network structure that provides for relatively unimpeded movement of the ions. This particulate network imparts mechanical stability to the electrolyte but plays no part in ion transport. In contrast, the Li–hectorite filler plays an active role in ion transport since the relatively large platelets serve as the anion and allow for exceptionally large Li transference numbers. While the hectorite also forms a self-supporting network, the morphology is less uniform and more contiguous than those obtained from fumed silica with most of the hectorite platelets displaying evidence of intercalation rather than exfoliation. The differences in the morphology of the two systems are reflected in their structural breakdown under shear in that the fumed silica shows a gradual yielding behavior whereas the hectorite system undergoes a sharp transition.

4. Experimental

Electrolyte Preparation: The lithium bis(trifluoromethanesulfonyl)imide (LiTFSI) salt, obtained from 3M Co. (St. Paul, MN), was dried under vacuum at 80 °C for 48 h before use, and PEGdm with $M_n = 250$ g mol^{-1} was purchased from Aldrich Chemicals (Milwaukee, WI) and dried over 4 Å molecular sieves (Fisher Scientific, Pittsburgh, PA) for 1 week. Hydrophobic fumed silica (Aerosil R805), with 50 % of its native Si–OH surface replaced by octyl (C_8H_{17}) groups [28], was supplied by Degussa (Akron, OH) and dried at 120 °C under vacuum for 5 days. While additional polymer electrolytes were prepared here to facilitate morphological analysis (described later in this section), most of the polymer electrolytes examined here employed the compounds listed above. These compounds were routinely stored and used in an Ar-filled glove box maintained at a moisture level of < 5 ppm.

The fumed silica nanocomposite electrolytes were prepared by first dissolving a predetermined quantity of Li salt in PEGdm. The fumed silica particles were then added to the salt solution and dispersed with a high-shear BioSpec mixer (BioSpec Products, Bartlesville, OK) equipped with a rotor measuring 7 mm in diameter. The nanocomposite electrolyte was subsequently degassed under vacuum for 1 h to remove bubbles. The maximum moisture content in the material was < 50 ppm, according to a Karl–Fischer titration. Synthetic Na–hectorite (SKS-21, 88 meq./100 g, ~ 250 nm mean size, clay platelet anionic charge of ~ 60 000) was provided by Hoechst (Strasbourg, France). The ethylene carbonate (EC) was obtained from Aldrich Chemicals and dried in identical fashion as the PEGdm. The procedures for generating Li-exchanged hectorite and preparing nanocomposite electrolytes with exfoliated Li–hectorite initially involved converting native hectorite to Li–hectorite via serial mixing with LiCl in deionized water, followed by centrifugation and drying in a conventional oven [30]. The resultant dry Li–hectorite powder was then dispersed in a high-dielectric solvent by a Silverson high-shear mixer. In the present work, nanocomposites were produced with a mixture of dry EC and dry PEGdm (1:1 v/v) as the mixed solvent. The final Li–hectorite nanocomposites retained a water content of ca. 200–300 ppm.

Electrochemistry: An EG&G Princeton Applied Research (PAR) 273 potentiostat and PAR 5210 lock-in amplifier controlled by the PAR M398 impedance software was used to measure electrolyte conductivity by alternating current (AC) impedance spectroscopy. The temperature was controlled to within ± 0.5 °C using a Fisher Isotemp 1016S circulating water bath. Conductivity cells with Pt wire electrodes were used [29,30]. Lithium-ion transference numbers were measured by two different methods. Electrophoretic nuclear magnetic resonance (ENMR) spectroscopy was performed on the fumed silica nanocomposite electrolytes according to the methodology prescribed by Dai and Zawodzinski [38] and Walls and Zawodzinski [39]. In this analysis, a sample was placed in an electric field during pulse field gradient NMR (pfg-NMR) so that the migration of cations or anions (depending on the nucleus of interest) could be probed and related to the transference number. The steady-state current method of Bruce and Vincent [40] was used to examine the Li–hectorite nanocomposite electrolytes [30].

Rheology: Dynamic rheological tests were performed with a Rheometrics Dynamic Stress Rheometer (DSR II) in which the test geometry temperature was controlled by a Polyscience recirculating bath filled with a 50:50 v/v mixture of water and ethylene glycol. Several different test geometries were used according to sample and test requirements: 40 mm cone and plate (cone angle of 0.05 rad), 40 mm parallel plates with a ridged (serrated) surface, 25 mm cone and plate (cone angle of 0.1 rad), and 25 mm serrated plates. A Rheometrics RMS 800 strain-controlled rheometer was employed to measure the dynamic rheology of the Li–hectorite electrolytes. In this case, a single test geometry consisting of 25 mm parallel plates with a 1 mm sample gap was used. All measurements were acquired at ambient temperature (~ 20 °C). Dynamic frequency (ω) tests were performed safely within the limits of instrument sensitivity and the linear viscoelastic (LVE) regime of each sample. Dynamic stress (τ) tests were conducted with parallel (serrated, when appropriate) plates at ω values of 1 rad s^{-1} on the DSR II and 5 rad s^{-1} on the RMS 800 to extract values of the dynamic storage modulus (G').

Microscopy: Due to the deformable nature of the nanocomposite electrolytes generated here, homologous sample series were prepared for transmission electron microscopy (TEM) in which PEGdm was substituted partially or completely by PEG diacrylate (PEGda) from Aldrich Chemicals. The PEGda could be

ADVANCED FUNCTIONAL MATERIALS

chemically crosslinked in the presence of AIBN (Aldrich Chemicals) at 80 °C to form a material possessing greater solid-like character. Fumed silica nanocomposites were produced with 10 wt.-% Aerosil R711 (Degussa), which possesses cross-linkable methacrylate surface groups but the same primary particle size and surface area as R805, in various PEGdm/PEGda solutions. The Li–hectorite nanocomposite electrolytes were prepared over a concentration range of 0.25–1.00 M Li^+ (approximately 20–50 wt.-% Li–hectorite) in a 1:1 v/v mixture of EC and PEGda. In all cases, the crosslinked materials were sectioned at –100 °C in a Reichert–Jung cryo-ultramicrotome, and the electron-transparent sections were imaged at 80 kV and various energy-loss (ΔE) settings with a Zeiss EM902 electron spectroscopic microscope.

Received: January 9, 2003

[1] F. B. Dias, L. Plomp, B. J. Veldhuis Jakobert, *J. Power Sources* **2000**, *88*, 169.
[2] F. M. Gray, *Solid Polymer Electrolytes*, VCH, New York **1991**.
[3] W. H. Meyer, *Adv. Mater.* **1998**, *10*, 439.
[4] E. Quartarone, P. Mustarelli, A. Magistris, *Solid State Ionics*, **1998**, *110*, 1.
[5] J. Y. Song, Y. Y. Wang, C. C. Wan, *J. Power Sources* **1999**, *77*, 183.
[6] J.-M. Tarascon, M. B. Armand, *Nature* **2001**, *414*, 359.
[7] Y. Nishi, *J. Power Sources* **2001**, *100*, 101.
[8] M. Doyle, T. F. Fuller, J. Newman, *Electrochim. Acta* **1994**, *39*, 2073.
[9] B. Kumar, L. G. Scanlon, *J. Electroceram.* **2000**, *5*, 127.
[10] A. S. Best, J. Adebahr, P. Jacobsson, D. R. MacFarlane, M. Forsyth, *Macromolecules* **2001**, *34*, 4549.
[11] F. Croce, G. B. Appetecchi, L. Persi, B. Scrosati, *Nature* **1998**, *394*, 456.
[12] F. Croce, R. Curini, A. Martinelli, L. Persi, F. Ronci, B. Scrosati, R. Caminiti, *J. Phys. Chem. B* **1999**, *103*, 10 632.
[13] F. Croce, L. Persi, B. Scrosati, *Solid State Ionics* **2000**, *135*, 47.
[14] F. Croce, L. Persi, B. Scrosati, F. Serraino-Fiory, E. Plichta, H. M. A., *Electrochim. Acta* **2001**, *46*, 2457.
[15] M. Forsyth, D. R. MacFarlane, A. S. Best, J. Adebahr, P. Jacobsson, A. J. Hill, *Solid State Ionics* **2002**, *147*, 203.
[16] H. Chen, F. Chang, *J. Polym. Sci. B: Polym. Phys.* **2001**, *39*, 2407.
[17] M. M. Doeff, J. S. Reed, *Solid State Ionics* **1998**, *113–115*, 109.
[18] W. Krawiec, L. G. Scanlon, J. P. Fellner, R. A. Vaia, S. Vasudevan, E. P. Giannelis, *J. Power Sources* **1995**, *54*, 310.
[19] S. Wong, R. A. Vaia, E. P. Giannelis, D. B. Zax, *Solid State Ionics* **1996**, *86–88*, 547.
[20] J. O. M. Bockris, A. K. N. Reddy, *Modern Electrochemisty 1: Ionics*, 2nd ed., Plenum Press, New York **1998**, Vol. 1.
[21] F. M. Gray, *Polymer Electrolytes*, Royal Society of Chemistry, Cambridge **1997**.
[22] R. A. Robinson, R. H. Stokes, *Electrolyte Solutions*, 2nd ed., Butterworths Scientific Publications, London **1959**.
[23] K. Hayamizu, Y. Aihara, S. Arai, C. G. Martinez, *J. Phys. Chem. B* **1999**, *103*, 519.
[24] J. Shi, C. A. Vincent, *Solid State Ionics* **1993**, *60*, 11.
[25] S. A. Khan, G. L. Baker, S. Colson, *Chem. Mater.* **1994**, *6*, 2359.
[26] S. R. Raghavan, M. W. Riley, P. S. Fedkiw, S. A. Khan, *Chem. Mater.* **1998**, *10*, 244.
[27] H. J. Walls, J. Zhou, J. A. Yerian, P. S. Fedkiw, S. A. Khan, M. K. Stowe, G. L. Baker, *J. Power Sources* **2000**, *89*, 156.
[28] S. R. Raghavan, J. Hou, G. L. Baker, S. A. Khan, *Langmuir* **2000**, *16*, 1066.
[29] J. Fan, P. S. Fedkiw, *J. Electrochem. Soc.* **1997**, *144*, 399.
[30] M. W. Riley, P. S. Fedkiw, S. A. Khan, *J. Electrochem. Soc.* **2002**, *149*, A667.
[31] C. W. Macosko, *Rheology: Principles, Measurements, and Applications*, VCH, New York **1994**.
[32] *Energy-Filtering Transmission Electron Microscopy* (Ed: L. Reimer), Springer-Verlag, Heidelberg **1995**.
[33] A. Du Chesne, *Macromol. Chem. Phys.* **1999**, *200*, 1813.
[34] T. C. Merkel, B. D. Freeman, R. J. Spontak, Z. He, A. Morisato, I. Pinnau, P. Meakin, A. J. Hill, *Science* **2002**, *296*, 519.
[35] K. E. Thomas, S. E. Sloop, J. B. Kerr, J. Newman, *J. Power Sources* **2000**, *89*, 132.
[36] M. W. Riley, *Ph.D. Thesis*, North Carolina State University, Raleigh, NC **2002**.
[37] R. J. Spontak, unpublished.
[38] H. Dai, T. A. Zawodzinski, Jr, *J. Electrochem. Soc.* **1996**, *143*, L107.
[39] H. J. Walls, T. A. Zawodzinski, Jr, *Electrochem. Solid-State Lett.* **2000**, *3*, 321.
[40] P. G. Bruce, C. A. Vincent, *J. Electroanal. Chem.* **1987**, *225*, 1.

